

# Environmental Science Nano

Accepted Manuscript



This is an *Accepted Manuscript*, which has been through the Royal Society of Chemistry peer review process and has been accepted for publication.

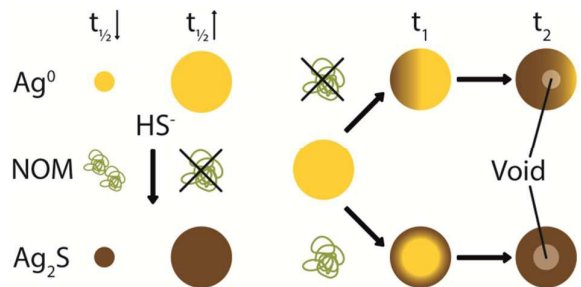
*Accepted Manuscripts* are published online shortly after acceptance, before technical editing, formatting and proof reading. Using this free service, authors can make their results available to the community, in citable form, before we publish the edited article. We will replace this *Accepted Manuscript* with the edited and formatted *Advance Article* as soon as it is available.

You can find more information about *Accepted Manuscripts* in the [Information for Authors](#).

Please note that technical editing may introduce minor changes to the text and/or graphics, which may alter content. The journal's standard [Terms & Conditions](#) and the [Ethical guidelines](#) still apply. In no event shall the Royal Society of Chemistry be held responsible for any errors or omissions in this *Accepted Manuscript* or any consequences arising from the use of any information it contains.

## Graphical Abstract

Humic acid increases the sulfidation rate of Ag-NP and leads to the formation of hollow spheres via the Kirkendall effect)



## Nano Impact

Silver nanoparticles (AgNP) are of ecotoxicological concern. The sulfidation of AgNP observed in urban wastewater systems and in wetlands reduces their toxicity by several orders of magnitudes. However, the sulfidation rate and the influence of humic acid (HA) on the sulfidation are still poorly understood. We show that the sulfidation rate increases with decreasing AgNP diameter and increasing HA concentrations. We reveal that the sulfidation of AgNP leads to the initial formation of  $\text{Ag}_2\text{S} - \text{Ag}^0$  core shell structures. Outward diffusion of Ag from the metallic core results in the formation of hollow  $\text{Ag}_2\text{S}$  NP by the Kirkendall effect.



## Environmental Science: Nano

## ARTICLE

## Effect of Humic Acid on the Kinetics of Silver Nanoparticle Sulfidation

Received 00th January 20xx,  
Accepted 00th January 20xx

Basilius Thalmann<sup>a,b</sup>, Andreas Voegelin<sup>a</sup>, Eberhard Morgenroth<sup>a,b</sup> and Ralf Kaegi<sup>a,†</sup>

DOI: 10.1039/x0xx00000x

www.rsc.org/

The sulfidation of metallic silver nanoparticles (AgNP) observed in urban wastewater systems and in natural waters reduces their toxicity by several orders of magnitude. However, the reaction rate of this transformation is only poorly understood and the influence of humic acid (HA) on AgNP sulfidation has not been studied to date. We therefore investigate the sulfidation kinetics of AgNP reacted with bisulfide (HS<sup>-</sup>) in the absence and presence of HA and evaluate different kinetic models to describe the observed reaction kinetics.

Citrate-stabilized AgNP of different sizes (20 – 200 nm) were reacted with an excess of HS<sup>-</sup> in the absence of HA as well as at HA concentrations ranging from 50 to 1000 mg L<sup>-1</sup>. The extent of AgNP sulfidation after selected reaction times was determined by X-ray absorption spectroscopy (XAS). The overall sulfidation rate increased with decreasing AgNP size and increasing HA concentration. The sulfidation rate of the AgNP was best described by a diffusion-limited solid-state reaction model (parabolic rate law). The corresponding half-life times of the AgNP ranged from minutes to hours. The increase of the sulfidation rate with increasing HA concentration may be explained by the adsorption of HA onto the AgNP surface facilitating the access of HS<sup>-</sup> to the particle surface. Results from analytical transmission electron microscopy suggest that the AgNP sulfidized asymmetrically in the absence of HA. In the presence of HA, initially formed concentric core-shell Ag<sup>0</sup>-Ag<sub>2</sub>S structures developed into hollow Ag<sub>2</sub>S nanoparticles with increasing reaction time, possibly via the Kirkendall effect.

## Introduction

Silver nanoparticles (AgNP) are widely applied to consumer products (e.g., textiles and cosmetics),<sup>1</sup> with the intention to slowly release antimicrobial active Ag<sup>+</sup>.<sup>2, 3</sup> During the use and the washing of such products, AgNP can detach from the host material<sup>4-6</sup> and may reach the aquatic environment causing environmental concern.<sup>7</sup> Mass flow analysis revealed, that the largest fraction of AgNP released will be discharged into urban wastewater systems<sup>8</sup> and about 5% will pass the wastewater treatment plants and reach surface waters.<sup>9</sup>

Released AgNP will interact with various constituents such as natural organic matter (NOM) present in the aquatic environment. Humic acid (HA), a part of NOM, was shown to

increase the colloidal stability of AgNP due to the attachment of HA onto the particles surface.<sup>10</sup> Additionally, the adsorption of HA onto the AgNP surface can reduce the toxicity of the AgNP.<sup>11</sup>

The environmentally most important AgNP transformations are the dissolution of AgNP and the formation of Ag<sub>2</sub>S, AgCl or Ag complexes with organics. In the presence of HA and light, the formation of smaller AgNP has been reported.<sup>12-14</sup> Dissolution is dependent on the size and the coating of the AgNP in addition to pH and dissolved molecular oxygen.<sup>15-18</sup> In chloride-rich environments, the dissolution of AgNP is followed by the precipitation of AgCl or the formation of soluble chloride complexes.<sup>19</sup> In the presence of sulfides, the formation of Ag<sub>2</sub>S is dominant due to its low solubility product.<sup>20</sup> In sulfidation experiments, HS<sup>-</sup> reacting with AgNP decreased faster with decreasing particle diameter and in the presence of HA, but these qualitative observations were not explored in more detail.<sup>21</sup>

In urban wastewater the sulfidation of AgNP to Ag<sub>2</sub>S starts in the sewer system<sup>22, 23</sup> and continues in the wastewater treatment plant due to elevated HS<sup>-</sup> concentrations.<sup>9, 24-27</sup> Within typical hydraulic residence times in the urban wastewater system of ~24 h, metallic AgNP get almost completely sulfidized. The sulfidation of AgNP has also been reported in freshwater wetland sediment.<sup>28</sup> We recently showed that AgNP sulfidation also occurs in oxic surface

<sup>a</sup> Eawag, Swiss Federal Institute of Aquatic Science and Technology, Überlandstrasse 133, CH-8600 Dübendorf

<sup>b</sup> ETH Zürich, Institute of Environmental Engineering, CH-8093 Zürich, Switzerland

† Corresponding author: ralf.kaegi@eawag.ch

Electronic Supplementary Information (ESI) available: Additional supportive information is provided for the AgNP characterization (Table S1, Figure S1 and Figure S2), XANES (Figure S3) and EXAFS (Figure S4) spectra, comparison of LCF derived Ag fractions from XANES and EXAFS (Figure S5), fits of the parabolic rate model to the data (Figure S6), AgNP size measurement over time (Figure S7), HR-TEM image of partly sulfidized 20-nm AgNP (Figure S8), SE image of 100-nm AgNP (Figure S9), TEM time sequence of 100-nm AgNP (Figure S10), SE and HAADF image of 100-nm AgNP (Figure S11), run table (Table S2), LCF results (Table S3) and rate coefficients (Table S4). See DOI: 10.1039/x0xx00000x

## ARTICLE

## Environmental Science: Nano

waters by reaction with metal sulfides such as ZnS and CuS with lower thermodynamic stability than Ag<sub>2</sub>S.<sup>29</sup> The toxicity of very poorly soluble Ag<sub>2</sub>S is several orders of magnitude lower than the toxicity of soluble Ag salts and the oxidation of Ag<sub>2</sub>S in oxic waters proceeds rather slowly.<sup>19, 30-32</sup> Furthermore, substantial amounts of HA are present in wastewater, as up to 85 mg organic C per g sewage sludge have been reported.<sup>33</sup> Despite the overarching importance of the sulfidation of AgNP and the ubiquitous presence of HA, the dependence of the sulfidation rates on the AgNP size and the HA concentrations is only poorly understood.<sup>21, 29, 34, 35 36</sup>

The objectives of this study were, therefore, to investigate the sulfidation kinetics and mechanism of AgNP reacting with HS<sup>-</sup> under oxic conditions and to determine the influence of HA on the sulfidation rates and mechanisms. We investigated the effects of AgNP (nominal) size (20, 40, 100 and 200 nm) and HA concentrations (0, 50, 250, 1000 mg<sub>HA</sub> L<sup>-1</sup>) on the sulfidation rates. The reaction progress was monitored by measuring the Ag speciation at selected reaction times using X-ray absorption spectroscopy (XAS). We evaluated four different kinetic models to best describe the sulfidation kinetics. Further insights into the reaction mechanism were obtained by transmission electron microscopy (TEM) analysis of partially and fully sulfidized AgNP.

## Materials and Methods

### Starting Materials

Citrate stabilized AgNP (20, 40, 100 and 200 nm in diameter; Nanocomposix, 1000 mg<sub>Ag</sub> L<sup>-1</sup>, BioPure, CA, USA) were used for all experiments. The particles were characterized using transmission electron microscopy (TEM), dynamic light scattering (DLS), phase analysis light scattering (PALS) and UV/Vis spectroscopy. The zeta potential was calculated from the electrophoretic mobility (PALS) using the Smoluchowski approximation. DLS and electrophoretic mobility measurements were performed with a Zetasizer (NanoZS, Malvern Instruments, UK). The plasmon resonance was recorded with a UV/Vis-spectrometer (Cary 100, Varian). The results are given in the supporting information (SI) and are in good agreement with the data provided by the supplier (Figure S1 and S2, Table S1).

For the sulfidation experiments, 56.4 mg of sodium hydrogen sulfide (NaHS, Alfa Aesar) were dissolved in 10 mL deionized water (doubly deionized (DDI) water was used in all experiments; Millipore, 18.2 MΩ cm) to obtain a bisulfide (HS<sup>-</sup>) stock solution of ~100 mM. The HS<sup>-</sup> concentration (100.4 mM) was determined iodometrically (according to Eaton, et al.<sup>37</sup>). In brief, 1 mL of lugol's solution was mixed with 50 mL of water and 20 μL stock solution followed by the addition of 1 mL of starch solution (10 g L<sup>-1</sup>). This solution was titrated with thiosulfate (3.26 mM) until it became colorless.

Humic acid (HA, Sigma Aldrich, Lot: #STBD5313V, technical grade) was used as received. A stock solution was produced by dissolving 70 mg HA in 50 mL DDI water. The iron concentration of the HA was 254 mmol<sub>Fe</sub> Kg<sub>HA</sub><sup>-1</sup> (measured by

inductively coupled plasma optical emission spectroscopy (ICP-OES) after acid digestion of 100 μL HA solution with 1 mL of HNO<sub>3</sub> (Ultrapure 60%, Merck, DE) and 100 μL H<sub>2</sub>O<sub>2</sub> (30%) in an UltraClave3 (MLS GmbH)).

### Methods

**AgNP Sulfidation Kinetic Experiments.** The kinetics of the reaction of AgNP with HS<sup>-</sup> and the influence of HA on the sulfidation rates were studied by mixing 20 μL of AgNP (final concentration: 100 ppm, 0.93 mM) with 175 μL buffer (50 mM, HEPES, pH 7.5) containing variable amounts of HA (0, 50, 250 or 1000 mg<sub>HA</sub> L<sup>-1</sup>) in a 500 μL Eppendorf tube. The sulfidation reaction was initiated by adding 5 μL of HS<sup>-</sup> stock solution (2.5 mM HS<sup>-</sup>). After selected reaction times the suspension was pipetted directly into the XAS sample holder and immediately frozen in liquid nitrogen to quench the reaction. Frozen samples were stored in liquid nitrogen until analyzed at the synchrotron (Table S2 summary of experiments conducted).

**Interaction of HA with AgNP and HS<sup>-</sup>.** The adsorption of HA to the AgNP was studied by mixing 30 μL AgNP stock solution (20, 40, 100 and 200 nm in diameter) with 270 μL of buffered HA mixture (50 mM HEPES, pH 7.5; 0, 25, 50, 100, 200, 400 or 800 mg<sub>HA</sub> L<sup>-1</sup>) and measuring the hydrodynamic diameter of the particles with DLS using a micro quartz cuvette (Portmann Instruments AG, CH). Additionally, the hydrodynamic diameter was recorded over 45 min for 20-nm AgNP with 0, 50 and 250 mg<sub>HA</sub> L<sup>-1</sup> in the presence of 2.5 mM HS<sup>-</sup>.

The interaction of HA with HS<sup>-</sup> was studied by reacting specific amounts of HS<sup>-</sup> (1 - 4.5 mM) with a buffered solution (pH = 7.5, 50 mM HEPES) containing 250 mg<sub>HA</sub> L<sup>-1</sup> in 1.5 mL Eppendorf tubes with minimal head space. An aliquot of 100 μL was used to determine the initial HS<sup>-</sup> concentration in every vial. The tubes were closed and sealed with Parafilm and the HA was separated by centrifugation (18'000 g, 60 min, Mikro 220R, Hettich Zentrifugen) at the end of the experiments. Additional experiments were conducted with 250 mg<sub>HA</sub> L<sup>-1</sup> and 2.3 mM HS<sup>-</sup> without centrifugation for the same time period (60 min). The HS<sup>-</sup> concentration in the supernatant / bulk solution was determined according to the methylene blue method (4500-S<sup>2-</sup>), as it is very selective to S<sup>2-</sup>.<sup>37</sup> In brief, 100 μL of sample was mixed with 0.9 mL of DDI water and 0.1 mL of N,N-Dimethylbenzene-1,4-diamine (337.5 mg (Sigma-Aldrich, CH) dissolved in 50 mL 49% H<sub>2</sub>SO<sub>4</sub>, 50 mM). This solution was reacted with 30 μL of an iron(III) chloride solution (9 M, FeCl<sub>3</sub>, Sigma-Aldrich, CH) for 4 min, followed by the addition of 0.32 mL of diammonium hydrogen phosphate (3.8 M, (NH<sub>3</sub>)<sub>2</sub>HPO<sub>4</sub>, Sigma-Aldrich, CH). The absorption peak maximum at 605 nm of the stoichiometrically formed dye methylene blue was measured with a photo spectrometer and the concentration was calculated using the extinction coefficient of ε = 132000 cm M<sup>-1</sup>.<sup>38</sup>

**Ag K-Edge X-ray Absorption Spectroscopy (XAS).** XAS was performed at the Ag K-edge (25'514 eV) at the Dutch Belgian Beamline (DUBBLE, BM01B) at the European Synchrotron Radiation Facility (ESRF, Grenoble, France). A closed-cycle He-cryostat adjusted to 80 K (DUBBLE) was used to cool the samples. The reference samples Ag<sub>0</sub> (metallic foil) and Ag<sub>2</sub>S

(acanthite) were measured in transmission mode. The frozen samples were measured with a 9-element monolithic Ge fluorescence detector (Canberra, CT, USA).

Athena<sup>39</sup> was used to process the X-ray absorption near-edge structure (XANES) and extended X-ray absorption fine structure (EXAFS) spectra and to quantify the metallic and the sulfidic fractions by linear combination fitting (LCF).  $E_0$  was set to 25'514 eV and a first-order polynomial fit to the data from 25'414 to 25'454 eV was subtracted from the raw data. A second-order polynomial fit to the data from 25'554 to 25'814 eV was used to normalize the edge-jump at  $E_0$  to unity and to flatten the spectrum. LCF analysis of the XANES spectra was performed over the energy-range from 25'494 to 25'814 eV, and LCF analysis of the EXAFS spectra over the  $k$ -range from 2.5 to 9 Å<sup>-1</sup>. The individual fractions of Ag<sup>0</sup> and Ag<sub>2</sub>S were constrained to values between 0 and 1, the sum was not constrained. The fractions of Ag<sup>0</sup> derived from the LCF analysis of the XANES and EXAFS data were averaged and are reported together with the respective standard deviations.

**Transmission Electron Microscopy.** Pristine, partially and fully sulfidized AgNP were characterized with a scanning transmission electron microscope (STEM, HD-2700-Cs, Hitachi, Japan). Samples for TEM analyses were prepared by either drop-on-grid deposition (Lacey-carbon Cu, Okenshoji Co. LTD, Japan) or direct on-grid centrifugation using carbon-coated copper grids (Quantifoil, DE).<sup>40</sup> Images were recorded using either a bright field (BF) or a high-angular annular dark field (HAADF) detector. High resolution images were processed using Digital Micrograph (v.1.85, Gatan). Elemental analysis of individual particles was performed using an energy dispersive X-ray detector (EDX) and the spectra were recorded and processed using Digital Micrograph.

## Results and Discussion

**Sulfidation Kinetics of AgNP.** A multi-factorial design (Table S2) was used to investigate the sulfidation kinetics of AgNP with HS<sup>-</sup> in the presence / absence of HA in oxic water. In time resolved experiments AgNP (20, 40, 100, 200 nm) were reacted with HS<sup>-</sup> (2.5 mM, HS<sup>-</sup> in fivefold excess compared to Ag) in the presence of HA (0, 50, 250, 1000 mg<sub>HA</sub> L<sup>-1</sup>) for up to 60 min and the reaction progress was monitored by determining the sulfidic and the metallic fraction of the suspension using Ag K-edge XAS. The recorded spectra and the corresponding LCF results for XANES (Figure S3) and EXAFS (Figure S4) analysis are given in the supporting information (SI, Table S3). In all experiments, the metallic fraction steadily decreased with increasing reaction time and the decrease was faster for smaller particles (Figure 1, Table S3). After 15 min reaction (1000 mg<sub>HA</sub> L<sup>-1</sup>) the 20- and 40-nm AgNP were almost completely sulfidized, whereas the 100- and 200-nm were still to 20 and 30 % metallic (Figure 1A). An increasing sulfidation rate (faster decrease of the metallic fraction) was observed for increasing HA concentrations at constant particle size (Figure 1B). After 15 min reaction time, the metallic fraction of the 20-nm AgNP decreased from 43% (absence of HA) over 27% (50

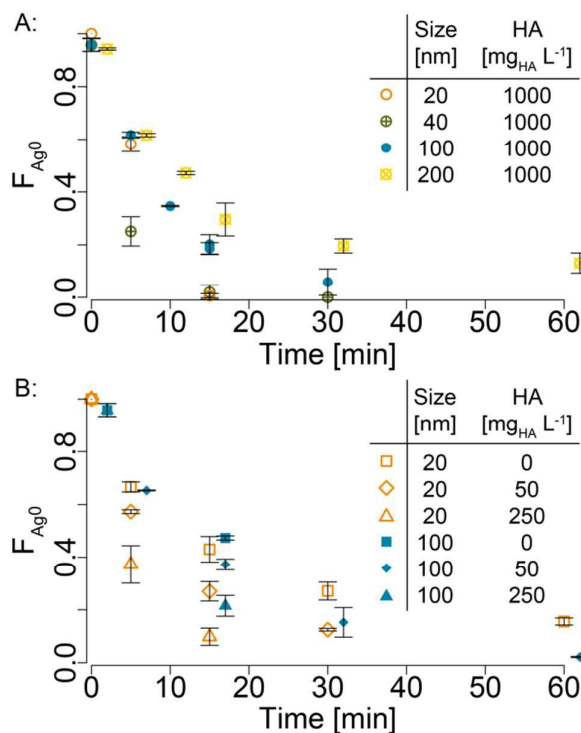


**Figure 1.** Average metallic Ag<sup>0</sup> fraction from LCF (XANES and EXAFS) against time for different experiments (error bars = 1σ, derived from average of XANES and EXAFS Ag<sup>0</sup> fraction, Table S3). The legend is given as inset. For better readability the data of the 200-nm AgNP have been shifted by plus 2 min. **A:** Different AgNP sizes at 1000 mg<sub>HA</sub> L<sup>-1</sup>, **B:** different HA concentrations (0, 50 and 250 mg<sub>HA</sub> L<sup>-1</sup>) for experiments with 20 and 100 nm AgNP. For better readability the data of the 100-nm AgNP have been shifted by plus 2 min.

mg<sub>HA</sub> L<sup>-1</sup>) and 10% (250 mg<sub>HA</sub> L<sup>-1</sup>) and was completed in the presence of 1000 mg<sub>HA</sub> L<sup>-1</sup>.

Four different models were evaluated to describe the sulfidation kinetics of AgNP: (i) A parabolic rate model originally proposed by Jander<sup>41</sup> (parabolic rate model, Eq. 1), which has previously been applied to describe the diffusion-limited solid state reaction of Ag<sup>0</sup> and Sulfur at elevated temperatures.<sup>42, 43</sup> (ii) A pseudo first-order rate model which has been used to describe the sulfidation kinetics of AgNP (FO model, Eq. 2).<sup>21</sup> (iii) A shrinking core model where the reaction progress is limited by diffusion through an outer, reacted (ash) layer (Ash model, Eq. 3).<sup>44</sup> (iv) A shrinking core model limited by the chemical reaction at the reactive surface of the shrinking core (Chem model, Eq. 4)<sup>44</sup>:

$$F = \left(1 - \sqrt{\frac{k}{r^2} \times t}\right)^3 \quad (\text{Eq. 1})$$

$$F = e^{-k \times t} \quad (\text{Eq. 2})$$

$$1 - 3F^{2/3} + 2F = \frac{k}{r^2} \times t \quad (\text{Eq. 3})$$

$$1 - F^{1/3} = \frac{k}{r} \times t \quad (\text{Eq. 4})$$

$F$  is the metallic Ag fraction (determined by XAS),  $r$  is the radius of the AgNP (determined by TEM),  $k$  is the rate constant and  $t$  is the time. All four models were fitted to the measured data using the non-linear regression package (nls2) for the statistic program R.<sup>45</sup>

Results of two selected time series (40 and 200 nm with 1000 mg<sub>HA</sub> L<sup>-1</sup>) are given for each model in Figure 2. Qualitatively, the parabolic rate and the FO model fitted the data better than the two other models. When comparing the model fits for the sulfidation of the 200-nm AgNP the parabolic rate model seemed to reproduce the measured data more closely than the FO model. The residual sum of squares (RSS) from each fitted data series was summed to compare the overall fit quality of the individual models. The Chem and Ash model had the highest values (0.70 and 0.44) followed by the FO model (0.19) and the parabolic rate model had the lowest value (0.15) indicating the best fit quality. Thus, qualitative visual inspection and the sum of RSS both suggested that the parabolic rate model was best suited to describe the sulfidation kinetics of AgNP (results of the model with the data is given in Figure S6 and Table S4). The experiment conducted with 20-nm AgNP in the presence 1000 mg<sub>HA</sub> L<sup>-1</sup> over 5 minutes showed an unusual high metallic fraction, which was considerably higher than the metallic fraction obtained for the 40 nm Ag-NP for the same treatment (Figure 1A). This high metallic fraction resulted in a substantial discrepancy between the model fit and the measured data for the 20-nm AgNP in

the presence of 1000 mg<sub>HA</sub> L<sup>-1</sup> (Figure S6A). As a consequence, a lower sulfidation rate was derived for the 20-nm AgNP compared to the 40-nm AgNP in the presence of 1000 mg<sub>HA</sub> L<sup>-1</sup> (Figure S6A). However, this apparently lower reaction rate is most probably due to an artifact in the experiment with 20-nm Ag-NP in the presence of 1000 mg<sub>HA</sub> L<sup>-1</sup> over 5 min (e.g., incomplete mixing of the AgNP with HA).

The parabolic rate model implies that the reaction is diffusion-limited and dependent on the concentration gradient of the diffusing element (given that sufficient HS<sup>-</sup> for the complete sulfidation of the AgNP is available). In the following, the rate coefficients derived from the parabolic rate model are evaluated in more detail with respect to the effects of nanoparticles size and HA concentration on sulfidation kinetics and mechanism.

In Figure 3 the sulfidation rate coefficients ( $k$ ) derived from the parabolic rate model are plotted against the HA concentration normalized to the total AgNP surface (HA<sub>norm</sub>, assuming ideal spherical particles). The rate coefficients increased almost linearly with increasing HA<sub>norm</sub>, except for the rate coefficients of 100-nm AgNP reacted with 0, 50 and 250 mg<sub>HA</sub> L<sup>-1</sup>, which had significantly higher  $k$  values. The  $k$  values for 100-nm AgNP reacted in the presence of 0 and 250 mg<sub>HA</sub> L<sup>-1</sup> were derived from only one time point (15 min) and are thus associated with a considerably higher uncertainty.

Possible explanations for the increasing rate constants with increasing HA<sub>norm</sub> are (i) the stabilizing effect of HA preventing

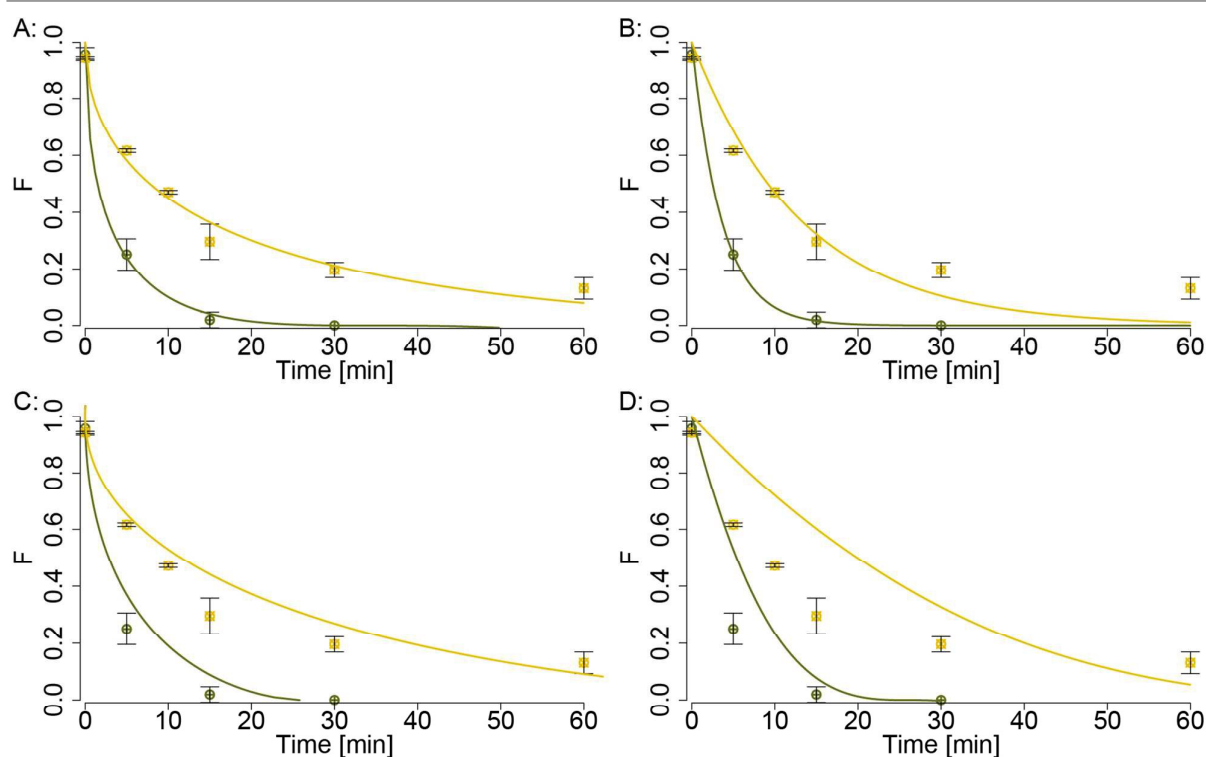


**Figure 2.** Comparison of the four different reaction models (A: parabolic rate model (Eq. 1), B: Pseudo-First-Order model (Eq. 2), C: Ash model (Eq. 3), D: Chem model (Eq. 4)) for two data series (green: 40-nm AgNP, yellow: 200-nm AgNP; both with 1000 mg<sub>HA</sub> L<sup>-1</sup>). Solid lines represent model fits derived from non-linear regressions to the experimental data.

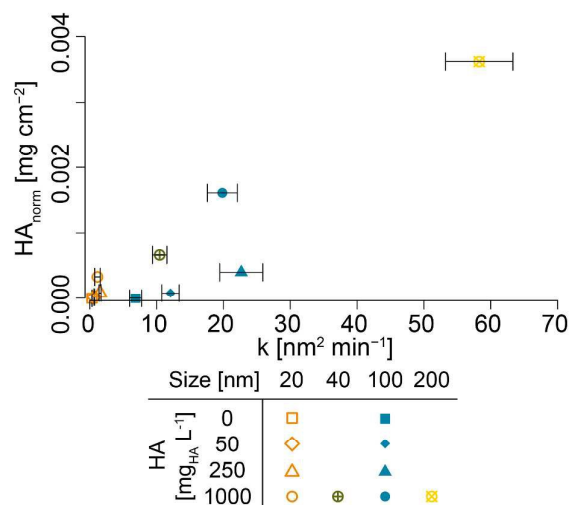


**Figure 3.** HA concentration divided by the total AgNP surface ( $HA_{norm}$ ) against sulfidation rates ( $k$ ) derived from the parabolic rate model ( $k$  values are given in Table S4, error bars =  $1\sigma$ ).

AgNP agglomeration and (ii) the replacement of citrate coating with HA leading to a larger AgNP surface area available for the sulfidation reaction, due to the presence of  $HS^-$  within the HA. The first hypothesis (i) was tested by measuring the hydrodynamic diameter of 20-nm AgNP (0, 50 or 250  $mg_{HA} L^{-1}$ ) during the reaction with  $HS^-$  over  $\sim 45$  min (Figure S7). In the absence of HA, the diameter increased from 32 to 42 nm and sedimentation was observed, indicating that agglomeration of AgNP induced by the sulfidation with  $HS^-$  occurred. In presence of HA, however, the diameter only increased by 2-4 nm regardless of the HA concentration. Thus, the stabilizing effect of HA may be responsible for an initial increase of the sulfidation rates (difference between absence and presence of HA), but with increasing HA concentrations no further stabilizing effect was observed. The increased reaction rates can thus not exclusively be explained with the colloidal stabilization of the AgNP by the HA.

To investigate the second hypothesis (ii) – replacement of citrate by HA bringing  $HS^-$  in close contact with the AgNP surface – we studied the interaction of HA with AgNP and HA with  $HS^-$ .

**Interaction of HA with AgNP.** The hydrodynamic diameter of

the AgNP in the presence of selected amounts of HA was measured by DLS (Table 1). The diameter of the 20-nm AgNP slightly decreased with the addition of 25  $mg_{HA} L^{-1}$  HA concentration but then steadily increased with increasing HA concentration to a maximum of 79 nm. The polydispersity index (PDI) followed the same trend with an initial slight decrease from 0.29 to 0.21 followed by a steady increase up to 0.836. However, the highest values might be unreliable due to the very high PDI of up to 0.84 (Table 1). Comparable results were obtained for experiments conducted with the 40-nm and the 100-nm AgNP, where the diameter increased to 63 nm and 117.7 nm with a PDI of 0.414 and 0.218 respectively. The hydrodynamic diameter of the 200-nm AgNP did not follow any consistent trend. The relative change in size for the 200-nm AgNP is expected to be even smaller than for the 100-nm AgNP and, therefore, may not be detectable with DLS anymore.

The initial decrease of the PDI indicates that the AgNP were stabilized by HA (and possibly disaggregated to some extent), leading to a more mono-disperse suspension, which also has been previously observed by other researchers.<sup>11, 46, 47</sup> The particle diameter mostly remained within 10% of the original value (determined in the absence of HA) for polydispersity index smaller than 0.3. Higher PDI were mainly observed at high HA concentrations and resulted in larger particle sizes. However, DLS results with a PDI  $> 0.3$  are difficult to interpret and are thus excluded from the discussion. Furthermore, additional measurements confirmed, that the particle size remained constant over 60 min, indicating a high colloidal stability of the suspensions. We did not observe a decreasing particle size with time as previously reported.<sup>12</sup> This apparent discrepancy can most likely be explained by the considerably shorter run times in our experiments (1 h) compared to the aforementioned study (24 h).

Although our DLS measurements did not allow us to assess whether citrate was displaced from the surface of the AgNP, it is generally assumed that citrate is only weakly bound to the AgNP surface. The stronger interaction of the AgNP surface with NOM, especially with sulfur and nitrogen groups in the form of thiols and amines, will lead to the displacement of citrate by NOM as suggested by Gunsolus, et al.<sup>11</sup> Furthermore, the high molecular weight fraction extracted

**Table 1.** Hydrodynamic Diameter of AgNP (100 ppm) with Different Concentrations of HA at pH 7.5.

| AgNP diameter [nm] <sup>1</sup> (PDI) <sup>2</sup> | 0 $mg_{HA} L^{-1}$ | 25 $mg_{HA} L^{-1}$ | 50 $mg_{HA} L^{-1}$ | 100 $mg_{HA} L^{-1}$ | 200 $mg_{HA} L^{-1}$ | 400 $mg_{HA} L^{-1}$ | 800 $mg_{HA} L^{-1}$ |
|--|--------------------|---------------------|---------------------|----------------------|----------------------|----------------------|----------------------|
| 20   | 29.3<br>(0.29)     | 27.3<br>(0.21)      | 27.7<br>(0.22)      | 31.1<br>(0.32)       | 37.9<br>(0.40)       | 55.8<br>(0.74)       | 79.1<br>(0.84)       |
| 40   | 39.4<br>(0.19)     | 38.4<br>(0.19)      | 39.8<br>(0.20)      | 40.3<br>(0.21)       | 43.3<br>(0.24)       | 49.6<br>(0.35)       | 63.3<br>(0.41)       |
| 100  | 103.7<br>(0.22)    | 98.6<br>(0.15)      | 96.3<br>(0.12)      | 98.2<br>(0.13)       | 108.1<br>(0.16)      | 116.2<br>(0.17)      | 117.7<br>(0.22)      |
| 200  | 228.8<br>(0.23)    | 254.3<br>(0.25)     | 233.2<br>(0.18)     | 242.4<br>(0.20)      | 233.9<br>(0.18)      | 213.4<br>(0.17)      | 235.8<br>(0.32)      |

<sup>1</sup>: The data refer to number weighted particle size distributions using the cumulant method.

<sup>2</sup>: PDI = Polydispersity Index

## ARTICLE

## Environmental Science: Nano

from a specific NOM source was shown to have stronger interactions with citrate coated AuNP compared to the lighter weight fraction.<sup>46, 47</sup> Thus, we assume that especially the heavy weight fraction of the NOM would displace the citrate from the AgNP surface, which would be in favour of hypothesis (ii). Whether the sorption of HA to the surface could increase the HS<sup>-</sup> concentration at the AgNP surface was therefore investigated in additional experiments.

**Interaction of HA with HS<sup>-</sup>.** Different concentrations of HS<sup>-</sup> were mixed with 250 mg<sub>HA</sub> L<sup>-1</sup>, followed by a centrifugal separation of the HA for 60 min. The HS<sup>-</sup> concentration was measured in the supernatant. The HS<sup>-</sup> associated with the HA, and thus removed by centrifugation, divided by the total HA concentration ( $q$ ) was plotted against the free HS<sup>-</sup> concentration measured in the supernatant ( $C$ , Figure 4). A Freundlich sorption isotherm was fitted to the data (Eq. 5):

$$q = l \times C^n \quad (\text{Eq. 5})$$

The two constants  $l$  and  $n$  were 0.00404(2) and 0.64(6) respectively (a standard error of  $1\sigma$  is given in brackets referring to the last digit). The sorption capacity of HA for metal cations is in the range of 0.1–0.2  $\mu\text{mol mg}_{\text{HA}}^{-1}$ ,<sup>48</sup> which is substantially lower compared to the observed sorption capacity of up to 7  $\mu\text{mol mg}_{\text{HA}}^{-1}$  for HS<sup>-</sup>. These high (apparent) sorption capacities may be explained by an oxidative loss of HS<sup>-</sup>, as it was recently shown that HS<sup>-</sup> can react with HA to form higher oxidized sulfur species.<sup>49</sup> However, the methylene blue method is specific to sulfides<sup>50</sup> and in experiments, where the HA was not separated by centrifugation, we did not observe a significant decrease of HS<sup>-</sup> over the time period of 60 min, and thus, the oxidative loss of HS<sup>-</sup> can be excluded. Alternatively, a fraction of HS<sup>-</sup> may have reacted with metals present in the HA and thus, may have precipitated as metal sulfides and removed during the centrifugation. Also this can be excluded, as ICP-OES measurement of the HA revealed only very small amounts of Fe (0.254  $\mu\text{mol}_{\text{Fe}} \text{mg}_{\text{HA}}^{-1}$ ), which could only explain a loss of 63.5  $\mu\text{mol}$  of HS<sup>-</sup> or 13% of the observed loss after centrifugation. Therefore, we speculate that due to the lower pKa of HA compared to HS<sup>-</sup>, the HS<sup>-</sup> becomes protonated within the Donnan volume to form H<sub>2</sub>S which may be sorbed to non-polar groups of the HA. The replacement of the citrate with HA and the sorption of HS<sup>-</sup> to HA may thus bring the sulfide close to the AgNP surface and could explain the increased sulfidation rates observed with increasing HA concentrations.

**Microscopic Insights into the Sulfidation Mechanism.** To study the mechanism of AgNP sulfidation in more detail, analytical STEM analyses were performed. Samples were collected from partially and fully sulfidized 20 and 100-nm AgNP after specific reaction times (5 and 45 min for 20-nm and 5 and 15 min or 4 h for 100-nm AgNP) in the absence and presence of HA (250 mg<sub>HA</sub> L<sup>-1</sup> for 20-nm and 1000 mg<sub>HA</sub> L<sup>-1</sup> for 100-nm particles, Figure 5, Table S2).

During sulfidation, the 20-nm AgNP aggregated to form larger colloids, as already suggested by the DLS experiments, but the primary particles preserved their shapes and remained

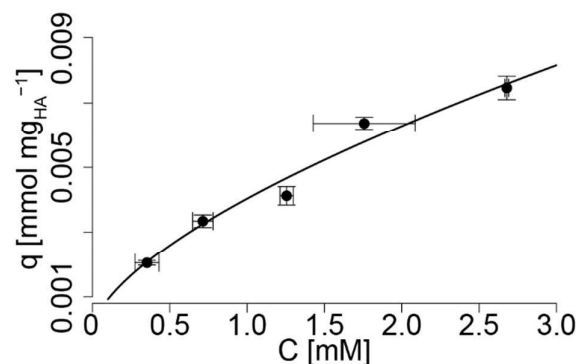
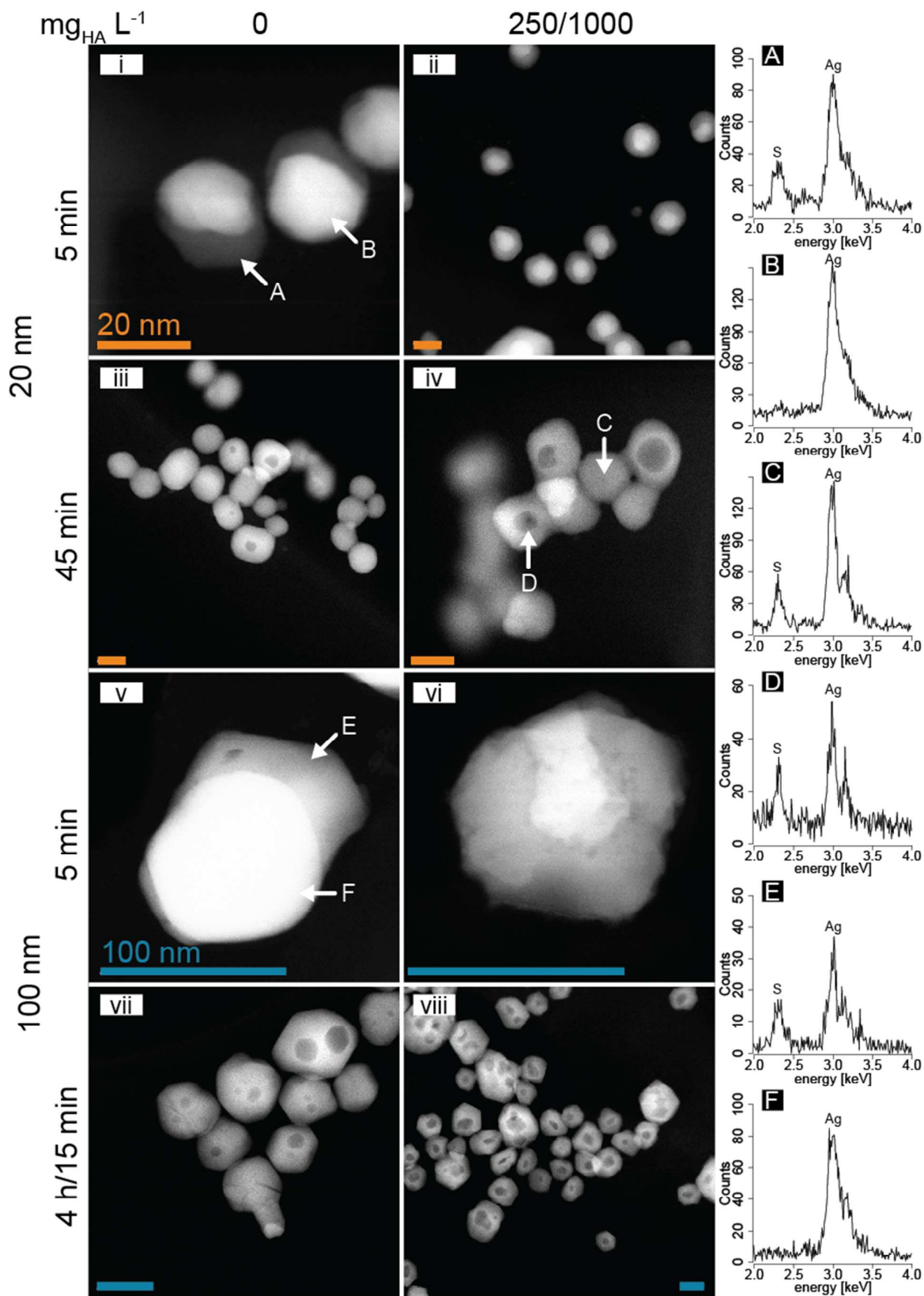


Figure 4. Adsorbed HS<sup>-</sup> on HA ( $q$ ) versus HS<sup>-</sup> in solution ( $C$ ) (for both values error bars ( $1\sigma$ ), derived from duplicate experiments). Sorption of HS<sup>-</sup> on HA follows a Freundlich isotherm (solid line, Eq. 5).

spherical. In the absence of HA and after 5 min, HAADF images of the 20-nm AgNP revealed a bright, spherical area with an adjacent grey sickle-shaped part. EDX analysis revealed that the bright part corresponded to metallic Ag and the grey areas represented Ag<sub>2</sub>S (Figure 5i, A, B). With increasing reaction time, the Ag<sub>2</sub>S increasingly replaced the metallic Ag resulting in mostly light-grey, spherical particles (Figure 5iii).

In the presence of 250 mg<sub>HA</sub> L<sup>-1</sup> and after 5 min reaction time, the metallic Ag (bright areas) was concentrically surrounded by a grey (Ag<sub>2</sub>S) shell, forming core-shell type structures (Figure 5ii, high resolution TEM image Figure S8). After 45 min reaction time, the contrast of the core-shell structures was reversed and a dark core was often surrounded by a light-grey shell. EDX analysis of the core and the shell revealed that both parts consisted of Ag<sub>2</sub>S (Figure 5iv, C, D).

For the 100-nm AgNP and in the absence of HA, the sulfidation resulted in similar structures as observed for the 20-nm AgNP (Figure 5v and vii). However, in the presence of 1000 mg<sub>HA</sub> L<sup>-1</sup>, the 100-nm AgNP developed more heterogeneous structures than without HA, with a distinct surface structure, probably representing adsorbed HA (Figure S9). Furthermore, we observed the reduction of freshly sulfidized AgNP to metallic Ag under the electron beam within a minute (Figure 5vi, a time sequence over one minute revealing the formation of metallic Ag under the electron beam is provided in SI, Figure S10). Well crystalline Ag<sub>2</sub>S particles are very stable under the electron beam as demonstrated by lattice fringes in high-resolution images (HR-TEM).<sup>32, 34</sup> Therefore, we speculate, that the presence of large amounts of HA (1000 mg L<sup>-1</sup>) interfered with the formation of well crystalline Ag<sub>2</sub>S nano particles and resulted in poorly crystalline Ag<sub>2</sub>S which was unstable under the electron beam. For the 100-nm AgNP, larger and in some cases even multiple dark spots were observed within a single particle (Figure 5vii and viii).



**Figure 5.** HAADF images of partially to fully sulfidized 20- and 100-nm AgNP in the absence and presence of HA (250 or 1000  $\text{mg}_{\text{HA}} \text{L}^{-1}$  for 20 and 100 nm AgNP, respectively) after 5, 15 and 45 min or 4 h (vii: 100 nm and 0  $\text{mg}_{\text{HA}} \text{L}^{-1}$ ) reaction time (orange bars are 20 nm (i-iv), blue bars are 100 nm (v-viii)). EDX spectra (right side, A - F) corresponding to specific locations in i, iv, and v are indicated by arrows.

The dark spots in the center of the sulfidized AgNP observed in Figure 5 could be explained by either different elemental compositions (e.g., lighter elements concentrated in the center) or by a reduced thickness.<sup>51</sup> Elemental analysis of the central dark spots revealed the same elemental distribution as for the rim of the particles. Therefore, the contrast observed on the HAADF image can only be explained by a thickness contrast. Additional secondary electron images (SE), probing the topography of the particles revealed that the sulfidized particles remained spherical (Figure S11). Therefore, the central dark spots observed in the HAADF images can only be explained by a central cavity.

The formation of hollow nanoparticles is well known in material science<sup>52-54</sup> and recently has also been described in environmental systems.<sup>55</sup> The formation of central voids can be explained by different diffusion coefficients of two counter-diffusing species across an interfacial layer, which is compensated by the (inward) diffusion of vacancies. When the concentration of the vacancies that migrated into the center of the particle reaches a certain threshold value, the vacancies collapse into a central cavity. This phenomena is known as Kirkendall-effect<sup>52</sup> and has been used to synthesize hollow Ag<sub>2</sub>Se nanoparticles in organic solvents.<sup>53</sup> We observed the formation of Kirkendall voids during the sulfidation of AgNP in oxic water, at room temperature and more prominently in the presence of HA. Furthermore, the 100-nm AgNP also had multiple voids within one particle, most likely due to the polycrystalline nature of larger AgNP. Similar core-shell structures as reported in this study may also have been observed by Impellitteri et al.<sup>27</sup> (Figure 3A and 4A in their publication) for AgNP that were sulfidized in real wastewater samples, indicating that Kirkendall-like core-shell structures may also form in real wastewater. The occurrence of hollow AgNP may therefore be indicative for the release of (engineered) AgNP into the wastewater.

In the Ag(0) – S(-II) system, presumably a thin layer of Ag<sub>2</sub>S initially forms and Ag diffuses faster through the Ag<sub>2</sub>S than S, which was previously also reported for bulk Ag(0) with S(0) at elevated temperatures (220° C).<sup>43</sup> These observations are in line with the parabolic rate model which is based on the assumption of diffusion limitation.

Furthermore, TEM analysis revealed, that in the absence of HA the sulfidation of AgNP mostly started from one side of the particle, whereas in the presence of HA the sulfidation resulted in more symmetrical core-shell structures. We hypothesize, that citrate was preventing the even sulfidation of the AgNP and the replacement of citrate with HA increased the reaction rate as an increased area of the particle surface was available for sulfidation, resulting in the observed core-shell structures. This hypothesis is also supported by the formation of larger and central Kirkendall voids that were generally observed in the presence of HA (20-nm AgNP). The ‘asymmetrical’ sulfidation observed in the absence of HA favors the formation of voids which are either off center or completely lost at the surface of the particles.

Results from the TEM investigations are thus in line with the hypothesis that the replacement of citrate coating with HA

increases the AgNP surface area available for the sulfidation. In addition, the adsorption of HS<sup>-</sup> within HA brings the HS<sup>-</sup> close to the AgNP surface and thus facilitates the sulfidation. The combination of both effects eventually led to increased sulfidation rates with increasing HA<sub>norm</sub> (Figure 3). The diffusion of S and Ag along subgrain boundaries<sup>29</sup> resulting in the formation of more heterogeneous structures observed for larger, poly-crystalline AgNP additionally increases the complexity of the sulfidation pathways of AgNP.

## Conclusions

The results of this study demonstrate that HA increases the sulfidation rates of AgNP. The half-life time ( $t_{1/2}$ , were 50 % of the total Ag was transformed to Ag<sub>2</sub>S) of AgNP was decreasing from 12 to 1 min with an increase of the HA concentration from 0 and 1000 mg<sub>HA</sub> L<sup>-1</sup> for the 20-nm AgNP. Based on the results from the current study, it is likely that the sulfidation of AgNP in the presence of HA is substantially accelerated and completed within one hour or less. The sulfidation of AgNP in the presence of HA initially led to the formation of core (Ag<sup>0</sup>) – shell (Ag<sub>2</sub>S) particles that transformed into hollow – Ag<sub>2</sub>S particles via the Kirkendall effect.

Furthermore, we found that the sulfidation kinetics are best described by a parabolic rate model, which implies that neither the overall Ag nor the HS<sup>-</sup> concentration influence the sulfidation rate. Therefore, in the presence of sufficient amounts of HS<sup>-</sup> to completely sulfidize all AgNP (which should be the case in urban wastewater systems)<sup>24, 56</sup> the half-life time of AgNP can be estimated based on their size and the concentrating of the HA in the respective water. The sulfidation of polycrystalline AgNP (100 nm) resulted in Ag<sub>2</sub>S particles that quickly degraded under the electron beam, in contrast to well-crystalline Ag<sub>2</sub>S generally formed in the absence of organics. This might indicate that Ag<sub>2</sub>S formed by sulfidation of Ag in the presence of HA is more reactive than Ag<sub>2</sub>S formed in the HA-free systems. Further work is required to evaluate this hypothesis and its potential implications for the assessment of the fate and impact of Ag in environmental systems.

## Acknowledgements

We acknowledge the Electron Microscopy Centers at ETH Zurich (EMEZ, Zurich, Switzerland) and at Empa (Swiss Federal Institute for Materials Science and Technology, Duebendorf, Switzerland) for providing access to the microscopes. The Swiss Norwegian Beamline at the European Synchrotron Radiation Facility (SNBL, ESRF, Grenoble, France) is acknowledged for the allocation of beamtime. We thank Dipanjan Banerjee for support at the Dutch Belgian Beamline (DUBBLE) at ESRF. This work is part of the project “Behavior of silver nanoparticles in a wastewater treatment plant” within the Swiss National Research Program NRP 64 “Opportunities and Risks of Nanomaterials”. Additionally, we would like to

thank Brian Sinnet for the support in the laboratories at Eawag.

## References

1. I. Woodrow Wilson, *Nanotechnology Consumer Products*, Informa Healthcare, 2015.
2. A. D. Russell and W. B. Hugo, *Progress in medicinal chemistry*, 1994, 31, 351-370.
3. H. T. Ratte, *Environmental Toxicology and Chemistry*, 1999, 18, 89-108.
4. J. Farkas, H. Peter, P. Christian, J. A. Gallego Urrea, M. Hasselov, J. Tuoriniemi, S. Gustafsson, E. Olsson, K. Hylland and K. V. Thomas, *Environ Int*, 2011, 37, 1057-1062.
5. L. Geranio, M. Heuberger and B. Nowack, *Environmental science & technology*, 2009, 43, 8113-8118.
6. T. Benn, B. Cavanagh, K. Hristovski, J. D. Posner and P. Westerhoff, *J. Environ. Qual.*, 2010, 39, 1875-1882.
7. F. Gottschalk, T. Sonderer, R. W. Scholz and B. Nowack, *Environmental science & technology*, 2009, 43, 9216-9222.
8. T. Y. Sun, F. Gottschalk, K. Hungerbühler and B. Nowack, *Environmental Pollution*, 2014, 185, 69-76.
9. R. Kaegi, A. Voegelin, B. Sinnet, S. Zuleeg, H. Hagendorfer, M. Burkhardt and H. Siegrist, *Environmental science & technology*, 2011, 45, 3902-3908.
10. Y. Yin, M. Shen, Z. Tan, S. Yu, J.-f. Liu and G. Jiang, *Environmental science & technology*, 2015, DOI: 10.1021/es5061287.
11. I. L. Gunsolus, M. P. S. Mousavi, K. Hussein, P. Bühlmann and C. L. Haynes, *Environmental science & technology*, 2015, DOI: 10.1021/acs.est.5b01496.
12. V. Manoharan, A. Ravindran and C. H. Anjali, *Cell Biochem Biophys*, 2014, 68, 127-131.
13. N. Akaighe, R. I. Maccuspie, D. A. Navarro, D. S. Aga, S. Banerjee, M. Sohn and V. K. Sharma, *Environmental science & technology*, 2011, 45, 3895-3901.
14. F. Maurer, I. Christl, M. Hoffmann and R. Kretzschmar, *Environmental science & technology*, 2012, 46, 8808-8816.
15. T. Peretyazhko, Q. Zhang and V. L. Colvin, *Environmental science & technology*, 2014, DOI: 10.1021/es5023202.
16. R. Ma, C. Levard, S. M. Marinakos, Y. Cheng, J. Liu, F. M. Michel, G. E. Brown and G. V. Lowry, *Environmental science & technology*, 2012, 46, 752-759.
17. W. Zhang, Y. Yao, N. Sullivan and Y. Chen, *Environmental science & technology*, 2011, 45, 4422-4428.
18. J. Liu and R. H. Hurt, *Environmental science & technology*, 2010, 44, 2169-2175.
19. C. Levard, S. Mitra, T. Yang, A. D. Jew, A. R. Badireddy, G. V. Lowry and G. E. Brown, Jr., *Environmental science & technology*, 2013, 47, 5738-5745.
20. W. M. Haynes, *CRC Handbook of Chemistry and Physics*, CRC Press, Boca Raton, Fla, 95 edn., 2014.
21. J. Liu, K. G. Pennell and R. H. Hurt, *Environmental science & technology*, 2011, 45, 7345-7353.
22. R. Kaegi, A. Voegelin, C. Ort, B. Sinnet, B. Thalmann, J. Krismer, H. Hagendorfer, M. Elumelu and E. Mueller, *Water Res*, 2013, 47, 3866-3877.
23. G. Brunetti, E. Donner, G. Laera, R. Sekine, K. G. Scheckel, M. Khaksar, K. Vasilev, G. De Mastro and E. Lombi, *Water Research*, 2015, 77, 72-84.
24. P. H. Nielsen, K. Raunkjær and T. Hvitved-Jacobsen, *Water Science and Technology*, 1998, 37, 97-104.
25. R. Ma, C. Levard, J. D. Judy, J. M. Unrine, M. Durenkamp, B. Martin, B. Jefferson and G. V. Lowry, *Environmental science & technology*, 2013, DOI: 10.1021/es403646x.
26. C. Doolette, M. McLaughlin, J. Kirby, D. Batstone, H. Harris, H. Ge and G. Cornelis, *Chemistry Central Journal*, 2013, 7, 1-18.
27. C. A. Impellitteri, S. Harmon, R. G. Silva, B. W. Miller, K. G. Scheckel, T. P. Luxton, D. Schupp and S. Panguluri, *Water Research*, 2013, 47, 3878-3886.
28. G. V. Lowry, B. P. Espinasse, A. R. Badireddy, C. J. Richardson, B. C. Reinsch, L. D. Bryant, A. J. Bone, A. Deonarine, S. Chae, M. Therezien, B. P. Colman, H. Hsu-Kim, E. S. Bernhardt, C. W. Matson and M. R. Wiesner, *Environmental science & technology*, 2012, 46, 7027-7036.
29. B. Thalmann, A. Voegelin, B. Sinnet, E. Morgenroth and R. Kaegi, *Environmental science & technology*, 2014, 48, 4885-4892.
30. E. Navarro, F. Piccapietra, B. Wagner, F. Marconi, R. Kaegi, N. Odzak, L. Sigg and R. Behra, *Environmental science & technology*, 2008, 42, 8959-8964.
31. B. C. Reinsch, C. Levard, Z. Li, R. Ma, A. Wise, K. B. Gregory, G. E. Brown, Jr. and G. V. Lowry, *Environmental science & technology*, 2012, 46, 6992-7000.
32. B. Thalmann, A. Voegelin, U. von Gunten, R. Behra, E. Morgenroth and R. Kaegi, *Environmental science & technology*, 2015, 49, 10911-10919.
33. V. Réveillé, L. Mansuy, É. Jardé and É. Garnier-Sillam, *Organic Geochemistry*, 2003, 34, 615-627.
34. C. Levard, B. C. Reinsch, F. M. Michel, C. Oumahi, G. V. Lowry and G. E. Brown, *Environmental science & technology*, 2011, 45, 5260-5266.
35. R. D. Kent, J. G. Oser and P. J. Vikesland, *Environmental science & technology*, 2014, 48, 8564-8572.
36. C. Levard, E. M. Hotze, B. P. Colman, A. L. Dale, L. Truong, X. Y. Yang, A. J. Bone, G. E. Brown, Jr., R. L. Tanguay, R. T. Di Giulio, E. S. Bernhardt, J. N. Meyer, M. R. Wiesner and G. V. Lowry, *Environmental science & technology*, 2013, 47, 13440-13448.
37. A. D. Eaton, M. A. H. Franson, A. P. H. Association, A. W. W. Association and W. E. Federation, *Standard Methods for the Examination of Water & Wastewater*, American Public Health Association, 2005.
38. J. Cenens and R. A. Schoonheydt, *Clays and Clay Minerals*, 1988, 36, 214-224.
39. B. Ravel and M. Newville, *Journal of Synchrotron Radiation*, 2005, 12, 537-541.
40. D. Mavrocordatos, C.-P. Lienemann and D. Perret, *Mikrochim Acta*, 1994, 117, 39-47.
41. W. Jander, *Zeitschrift für anorganische und allgemeine Chemie*, 1927, 163, 1-30.
42. I. Bartkovicz and A. Stokłosa, *Solid State Ionics*, 1987, 24, 45-49.
43. K. N. Strafford, *Metallurgical Reviews*, 1969, 14, 153-174.
44. O. Levenspiel, *Industrial & engineering chemistry research*, 1999, 38, 4140-4143.

## ARTICLE

Environmental Science: Nano

45. R. C. Team, *R: A Language and Environment for Statistical Computing*, R Foundation for Statistical Computing, 2012.
46. S. M. Louie, E. R. Spielman-Sun, M. J. Small, R. D. Tilton and G. V. Lowry, *Environmental science & technology*, 2015, 49, 2188-2198.
47. S. M. Louie, R. D. Tilton and G. V. Lowry, *Environmental science & technology*, 2013, 47, 4245-4254.
48. H. Kerndorff and M. Schnitzer, *Geochimica et Cosmochimica Acta*, 1980, 44, 1701-1708.
49. Z.-G. Yu, S. Peiffer, J. Göttlicher and K.-H. Knorr, *Environmental science & technology*, 2015, 49, 5441-5449.
50. J. Small and H. Hintelmann, *Analytical and Bioanalytical Chemistry*, 2007, 387, 2881-2886.
51. S. Utsunomiya and R. C. Ewing, *Environmental science & technology*, 2003, 37, 786-791.
52. W. Wang, M. Dahl and Y. Yin, *Chem Mater*, 2013, 25, 1179-1189.
53. Y. Tang and M. Ouyang, *Nat Mater*, 2007, 6, 754-759.
54. B. D. Anderson and J. B. Tracy, *Nanoscale*, 2014, 6, 12195-12216.
55. F.-A. Weber, A. Voegelin, R. Kaegi and R. Kretzschmar, *Nature Geosci*, 2009, 2, 267-271.
56. F. Gottschalk, T. Sonderer, R. W. Scholz and B. Nowack, *Environmental Toxicology and Chemistry*, 2010, 29, 1036-1048.